

# Study of the impact of the post-MS evolution of the host star on the orbits of close-in planets.★

## II. A giant planet in a close-in orbit around the RGB star HIP 63242

M. I. Jones<sup>1,2</sup>, J. S. Jenkins<sup>1</sup>, P. Rojo<sup>1</sup>, C. H. F. Melo<sup>2</sup>, and Paz Bluhm<sup>3</sup>

<sup>1</sup> Departamento de Astronomía, Universidad de Chile, Camino El Observatorio 1515, Las Condes, Santiago, Chile  
e-mail: mjones@das.uchile.cl

<sup>2</sup> European Southern Observatory, Casilla 19001, Santiago, Chile

<sup>3</sup> Departamento de Astronomía, Universidad de Concepción, Casilla 160-C, Concepción, Chile

### ABSTRACT

**Context.** More than 40 planets have been found around giant stars, revealing a lack of systems orbiting interior to  $\sim 0.6$  AU. This observational fact contrasts with the planetary population around solar-type stars and has been interpreted as the result of the orbital evolution of planets due to the interaction with the host star and/or because of a different formation/migration scenario of planets around more massive stars.

**Aims.** We are conducting a radial velocity study of a sample of 166 giant stars aimed at studying the population of close-in planets orbiting post-main sequence stars.

**Methods.** We have computed precision radial velocities from multi-epoch spectroscopic data, in order to search for planets around giant stars.

**Results.** In this paper we present the discovery of a massive planet around the intermediate-mass giant star HIP 63242. The best keplerian fit to the data lead to an orbital distance of 0.57 AU, an eccentricity of 0.23 and a projected mass of  $9.2 M_J$ . HIP 63242 b is the innermost planet detected around any intermediate-mass giant star and also the first planet detected in our survey.

**Key words.** Stars: horizontal-branch – Planet-star interactions

### 1. Introduction

So far, more than 800 exoplanets have been detected<sup>1</sup>, most of them by the radial velocity (RV) technique. The detection of planets by this method is strongly biased to solar-like host stars, having low rotational velocity and low levels of stellar activity (e.g. Jenkins et al. 2013). Fast rotation broadens the spectral lines, preventing us from computing precision RV variations, whereas stellar activity and spots produce spectral line asymmetries, which might mimic the doppler shift induced by a substellar companion (e.g. Queloz et al. 2001; Huelamo et al. 2008). In addition, very low mass stars are too cool and present strong molecular bands in their spectra, making the computation of precision RV's more difficult, so generally only the slowest rotators are targeted (see Jenkins et al. 2009; Barnes et al. 2012). On the other hand, main-sequence (MS) stars more massive than  $\sim 1.3 M_\odot$  (corresponding to spectral types earlier than  $\sim F5$ ) are too hot and rotate fast, thus leading to an optical spectrum dominated by few and broad absorption lines. However, after the MS, early type stars become cooler and rotate slower than their MS progenitors (e.g. Schrijver & Pols 1993; Rutten & Pylyser 1998), and hence present many narrow absorption lines in their optical spectra. Also, even though they exhibit a higher level of activity than solar-type stars, giants with B-V color  $< 1.2$  are

quite stable, and show a stellar jitter at the  $\sim 20 \text{ m s}^{-1}$  level (Sato et al. 2005; Hekker et al. 2006; Jones et al. 2013). Therefore, evolved stars present an ideal case where the RV technique can be applied to search for planets orbiting intermediate-mass stars ( $1.3 \lesssim M_\star/M_\odot \lesssim 3.0$ ) and to study the post-MS star-planet interactions.

To date,  $\sim 100$  exoplanets have been detected around post-MS stars (including subgiants), revealing different orbital properties when compared to the planetary population orbiting FGK dwarfs. Figure 1 shows the semimajor axis distribution versus the mass of the host stars for all of the known planets. The small black dots, blue stars and red filled circles correspond to MS, sub-giants and giants host stars, respectively. The red filled triangle shows the position of HIP 63242 b. From Figure 1 it is evident that there is a lack of close-in orbiting planets ( $a \lesssim 0.6$  AU) around giant stars<sup>2</sup>, whereas there are many short period planets around MS stars. This observational result suggests that close-in planets are destroyed by the large envelope of the host star during the red giant phase. This idea was predicted theoretically to be caused by the strong tidal interaction between the planet and the stellar envelope. As a result, planets orbiting interior to a given distance spiral inward and are subsequently engulfed by the host star (e.g. Siess & Livio 1999; Sato et al.

\* Based on observations collected at La Silla - Paranal Observatory under programs ID's 085.C-0557, 087.C.0476, 089.C-0524 and 090.C-0345.

<sup>1</sup> As of March, 2013. Source: <http://exoplanet.eu>

<sup>2</sup> There is only one known planet around giant stars interior to 0.6 AU. The planet is in a 16.2 days period orbit around a  $0.8 M_\odot$  Horizontal Branch star (Setiawan et al. 2010). However, there is no available parallax for the host star, and thus its mass and evolutionary status are quite uncertain.

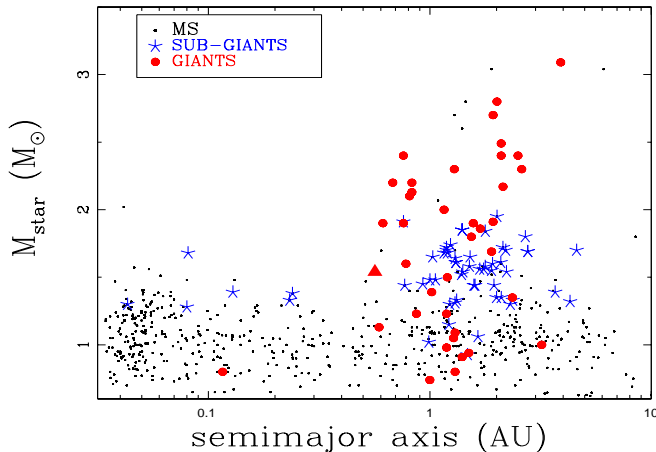


**Fig. 1.** Semimajor-axis distribution for planets around evolved stars. The blue stars and red filled circles correspond to sub-giant and giant host stars, respectively. The red triangle correspond to HIP 63242 b. For comparison, planets around MS stars are also plotted (small black dots).

2008; Villaver & Livio 2009; Kunitomo et al. 2011). However, the planetary population around subgiant stars shows a similar trend, i.e., a deficit of planets orbiting interior to  $\sim 0.6$  AU. Since subgiant stars still have relatively small radii, the tidal effect is not expected to significantly affect the planetary orbits, meaning that stellar evolution cannot be solely responsible for this observational result (Johnson et al. 2007). In fact, Bowler et al. 2010 showed that the period distribution of planets around intermediate-mass stars (all of them detected around subgiants) is different than the population of planets around FGK dwarfs, at the  $4\sigma$  level. In particular they found that planets around intermediate-mass stars present systematically larger semimajor axis, compared to planets orbiting low-mass stars. This result might explain in part the planet desert observed in Figure 1, but does not explain the lack of planets around giant stars with  $\sim 1.0 - 1.5 M_{\odot}^3$ .

In this paper we present the detection of a massive giant planet around HIP 63242, a nearby G8 giant star. Based on the best keplerian fit, the minimum mass of HIP 63242 b is  $9.2 M_{\text{J}}$  with an orbital period of 124.6 days, corresponding to a semimajor axis of  $a = 0.57$  AU. This is the closest planet detected around a first ascending red giant branch (RGB) star, and the second closest around a giant star, after HIP 13044 (Setiawan et al. 2010).

## 2. Observations and data reduction

The data were obtained using FEROS (Kaufer et al. 1999), mounted on the 2.2m telescope, at La Silla Observatory. The typical exposure time for the spectra was 210 seconds, leading to a  $S/N > 100$ . The extraction of the FEROS spectra was done with the ESO Data Reduction System (DRS), which is available for FEROS users. The DRS performs a bias subtraction, flat fielding, orders tracing and extraction. In addition, the scattered light is subtracted. The wavelength calibration was computed using 4 calibration lamps (one ThAr + one ThArNe, instead of the 12 standard calibrations) having different exposure times and intensities, which allows coverage of all of the spectral range ( $\sim$

<sup>3</sup> This result is also attributed to a target selection bias in giant stars RV surveys

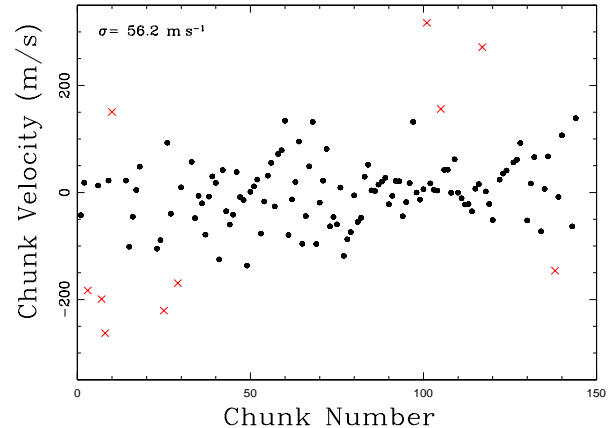


**Fig. 2.** Radial velocities computed to 144 different chunks, from a single observation of  $\tau$  Ceti. The solid black dots are the chunks velocities, while the red crosses correspond to the rejected velocities. The standard deviation is  $56.2 \text{ m s}^{-1}$ , corresponding to an error in the mean velocity of  $5.3 \text{ m s}^{-1}$ .

$3500 - 9200 \text{ \AA}$ ). The typical RMS in the wavelength solution is  $\sim 0.005 \text{ \AA}$ . Finally, the wavelength calibration is applied to the observed spectra, which are extracted order by order. Additionally, the reduction pipeline applies a barycentric correction to the extracted spectra, but this option was disabled because it retrieves the coordinates of the star that are recorded in the header, which are not accurate enough. Instead, this correction was computed separately, and then is applied to the reduced data, as discussed in the next section.

### 2.1. Radial velocity calculation

The RV's for each individual spectrum were measured in the following manner. Firstly, the doppler shift was computed by applying a Cross Correlation (Tonry & Davis 1979) between the stellar spectrum and its corresponding template (high S/N spectrum of the same star). For this purpose we used the IRAF task RV/fxcor (Fitzpatrick 1993). This method was applied to  $\sim 50 \text{ \AA}$  chunks (corresponding to  $\sim 1700$  pixels), leading to a total of 144 different RV's per observation. Then, for each dataset, the mean velocity was computed, rejecting in an iterative way every point lying more than  $2.5$  sigma from the mean, which typically corresponds to 20 % of them. It is worth mentioning that since all of the orders were included, cutting only 100 pixels at the edges, many chunks lead to very deviating velocities mainly either due to low S/N (specially toward the blue) or because of the presence of telluric lines (in the red part of the spectrum).

Figure 2 shows the chunk velocities from one spectrum of  $\tau$  Ceti<sup>4</sup>. The black dots are the non-deviant velocities and the red crosses are those rejected by the procedure just described (some of them are out of the plotting region). The standard deviation of the chunk velocities is  $56.2 \text{ m s}^{-1}$ , which corresponds to an error in the mean<sup>5</sup> of just  $5.3 \text{ m s}^{-1}$ . The second step consists of a similar procedure, but this time the cross correlation is computed between the simultaneous calibration lamp (sky fiber) and one

<sup>4</sup>  $\tau$  Ceti is a known stable star at the few  $\text{m s}^{-1}$  level. However, Tuomi et al. 2012, have shown that it hosts a planetary system

<sup>5</sup> The error in the mean is given by:  $\sigma/\sqrt{n_c}$ , where  $\sigma$  is the standard deviation of the chunks velocities and  $n_c$  is the number of non-rejected chunks used in the analysis

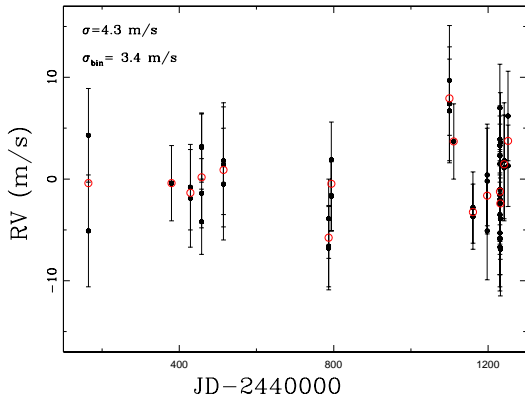


**Fig. 3.** Three years observations of the radial velocity standard star  $\tau$  Ceti. The black dots correspond to the RV's measured from individual FEROS spectra. The RMS is  $4.3 \text{ m s}^{-1}$ . The red open circles represent the binned RV's for individual nights. This time the RMS drops to  $3.4 \text{ m s}^{-1}$ .

of the lamps that was used for the wavelength calibration of that night (i.e., corresponding to the night zero point), having a similar exposure time to the simultaneous calibration lamp. This procedure is necessary to subtract the nightly drift, produced mainly by small variations in the refraction index of air in the spectrograph during the night, which at first order translates into a linear RV shift as large as  $\sim 150 \text{ m s}^{-1}$ . It is worth to mention that no second order correction was applied, like the RV shift between the two fibers, which is typically  $\sim 2\text{-}3 \text{ m s}^{-1}$  (Setiawan et al. 2000). Finally, the radial velocity for each epoch is computed by:

$$RV = RV_{\text{ob,tem}} + RV_{\text{drift}} + BC \quad (1)$$

where the first and second terms correspond to the RV computed for the object with its corresponding template and to the nightly drift, as explained above. The third term corresponds to the barycentric correction, which is computed using the mean time of the observation and using the actual coordinates of the star at that time, which are slightly different to the ones recorded in the image header (typically up to  $\sim 1\text{-}2$  arcminutes). This is quite important, since the error in the header coordinates translates into a RV uncertainty as big as  $\sim 5\text{-}10 \text{ m s}^{-1}$ . Finally, we tested the long-term precision of FEROS using 52 spectra of  $\tau$  Ceti, taken in 17 different nights (one spectrum was used as template) during the last three years. The resulting RV's are shown in Figure 3 (black dots). The measured RMS is  $4.3 \text{ m s}^{-1}$ . In addition, we binned the RV datapoints for individual nights, in order to average out the main stellar oscillations modes<sup>6</sup> (e.g. O'toole et al. 2008). The binned radial velocities (red open circles) lead to a RMS of only  $3.4 \text{ m s}^{-1}$ . This result shows the huge potential of FEROS for high precision RV studies of bright stars.

### 3. HIP 63242 b: the closest planet around and intermediate-mass giant star

According to the Hipparcos catalogue, HIP 63242 is a G8III star with  $V=6.87$ ,  $B-V=1.03$  and a parallax of  $\pi=7.42 \pm 0.49$ , which correspond to a distance of 135 pc. As for the rest of the stars in our sample, we derived  $T_{\text{eff}}$ ,  $[\text{Fe}/\text{H}]$  and  $\log g$  for HIP 63242,

**Table 1.** Stellar properties of HIP 63242

Parameter	Value
B - V (mag)	$1.02 \pm 0.02$
V (mag)	$6.86 \pm 0.01$
$\pi$ (mas)	$7.42 \pm 0.49$
$T_{\text{eff}}$ (K)	$4830 \pm 100$
$\log g$ ( $\text{cm s}^{-2}$ )	$2.53 \pm 0.2$
$[\text{Fe}/\text{H}]$ (dex)	$-0.31 \pm 0.09$
L ( $L_{\odot}$ )	$42.7 \pm 0.08$
Mass ( $M_{\odot}$ )	$1.54 \pm 0.05$
$v \sin i$ ( $\text{km s}^{-1}$ )	$3.7 \pm 0.1$

using the equivalent width of iron lines (Fe I and Fe II), by imposing excitation and ionization equilibrium. In order to do this we used the MOOG<sup>7</sup> code (Sneden 1973) along with the Kurucz (1993) atmosphere models. For a more detailed description see Jones et al. (2011). Additionally, we computed the luminosity of HIP 63242 using the bolometric corrections given in Alonso et al. (1999) and the 3-D extinction maps of Arenou et al. (1992). We compared the resulting  $T_{\text{eff}}$ ,  $[\text{Fe}/\text{H}]$  and stellar luminosity, which are listed in Table 1, with Salasnich et al. (2000) evolutionary models. We derived a mass of  $1.54 M_{\odot}$  for HIP 63242, using a linear interpolation method, as described in Jones et al. 2011. Figure 4 shows the position of HIP 63242 in the HR diagram and the closest evolutionary tracks from Salasnich et al. (2000) (upper panel). This star is clearly ascending the RGB, since no HB model cross its position in the HR diagram. For comparison, Figure 4 (lower panel) also shows two evolutionary isomass tracks taken from the Yonsei-Yale evolutionary models (Demarque et al. 2004) with solar-scaled metal abundances ( $[\alpha/\text{Fe}]=0.0$ ). Both tracks were interpolated to  $[\text{Fe}/\text{H}]=-0.31$ , using the interpolator included with the evolutionary models<sup>8</sup>. As can be seen, the mass for HIP 63242 derived using both sets of models is almost identical.

During the last three years, 16 spectra (including the template) of HIP 63242 were taken with FEROS. Its RV curve is shown in Figure 5. The resulting velocities are also listed in Table 3 (available in the electronic version). The error bars are  $\sim 5\text{-}8 \text{ m s}^{-1}$ , therefore are smaller than the symbol sizes. The best keplerian fit<sup>9</sup> is overplotted (solid black curve). It can be seen that there is a strong RV signal present in the data. The orbital parameters of the planet are listed in Table 2. The RMS of the fit is  $23.7 \text{ m s}^{-1}$ , which is mainly explained by stellar jitter. However, it is also possible that the presence of a second planet in the system produces a larger scatter from the single planet fit. Unfortunately, there are not enough observations yet to test this hypothesis.

## 4. Photometric and Line Profile Analysis

Intrinsic stellar phenomena, such as spots, magnetic activity or stellar oscillations, are known to produce periodic RV signal, that can mimic the doppler shift induced by a substellar companion (e.g. Queloz et al. 2001 Huelamo et al. 2008; Figueira et al. 2010). We performed three standard tests aimed at determine whether this is the case for HIP 63242. First, we analyzed the Hipparcos photometric data, which consists of a total of 142

<sup>7</sup> <http://www.as.utexas.edu/~chris/moog.html>

<sup>8</sup> [www.astro.yale.edu/demarque/yystar.html](http://www.astro.yale.edu/demarque/yystar.html)

<sup>9</sup> The keplerian solution was computed using the Systemic Console (Meschiari et al. 2009)

<sup>6</sup> The typical exposure time of the  $\tau$  Ceti spectra is  $\sim 10\text{-}30$  seconds.

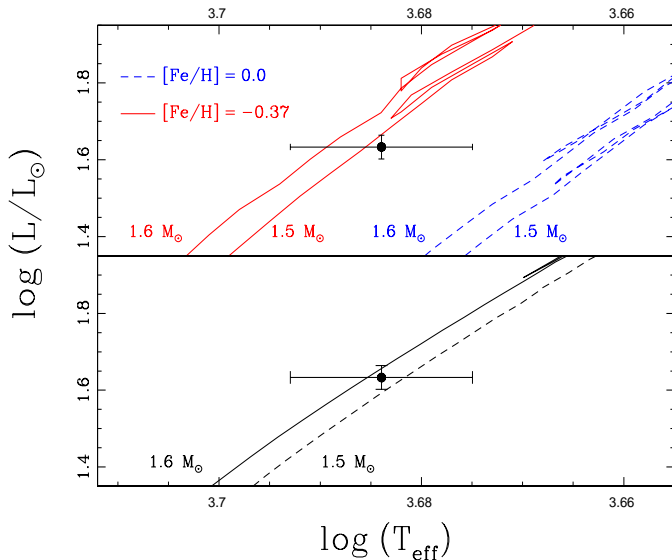


**Fig. 4.** Upper panel: Position of HIP 63242 in the HR diagram. The four closest evolutionary tracks from Salasnich et al. (2000) are overplotted. Lower panel: Same as for the upper panel, but this time using stellar tracks from the Yonsei-Yale database. Both models were interpolated to  $[\text{Fe}/\text{H}] = -0.31$ .

**Table 2.** Orbital parameters of HIP 63242 b

Parameter	Value
P (days)	124.6
K ( $\text{m s}^{-1}$ )	287.5
a (AU)	0.565
e	0.23
$\omega$ (deg)	118.2
$T_0$ (JD)	2455376.2
$M_p \sin i$	( $M_J$ ) 9.18

$H_p$  filter observations, taken between JD 2447869 and 2449013. The photometric data show a small dispersion of 0.009 mag, which cannot be responsible for the observed large RV variations. In fact, according to Hatzes (2002), a spot covering 5% of the stellar surface ( $\Delta m \sim 0.06$  mag) induces a RV variation below  $100 \text{ m s}^{-1}$ , on a star having a projected rotational velocity similar to HIP 63242 ( $v_{rot} = 3.6 \text{ km s}^{-1}$ ). Also, no significant periodic signal is observed in the Hipparcos photometry. Hence, rotational modulation can be discarded as the responsible mechanism for the observed RV signal. Also, we did a bisector analysis (Toner & Gray 1988), aimed at detecting asymmetries in the line profiles caused by intrinsic stellar phenomena. Figure 6 (upper panel) shows the bisector velocity span (BVS), which corresponds to the velocity difference between the bottom and the top of the CCF<sup>10</sup>, versus the observed radial velocities for HIP 63242. Clearly no obvious correlation between both quantities is present. Also, in the lower panel the width of the CCF as a function of the measured, RV's is plotted. Once again there is no correlation between both quantities. In both cases, the RMS around the mean is comparable to the errorbars. Finally, Figure 7 shows the S-index variations, computed in a similar fashion as described in Jenkins et al. (2008; 2011), against the observed

<sup>10</sup> We computed the average BVS from 11 different orders. The errorbars correspond to the error in the mean.

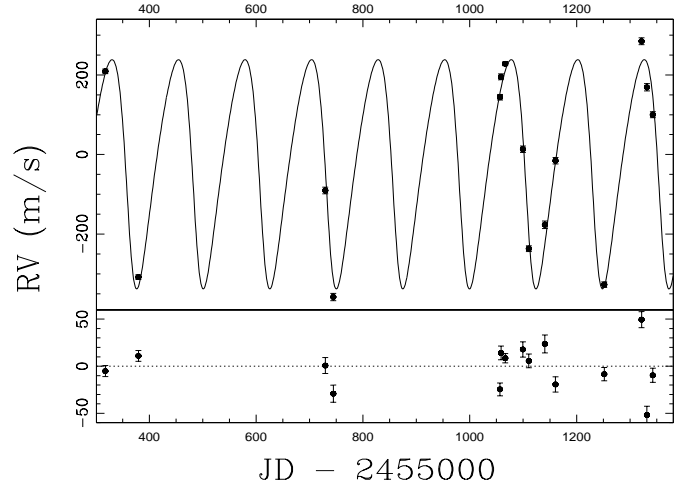


**Fig. 5.** RV curve for HIP 63242 (black dots). The best Keplerian fit is overplotted (black solid line).

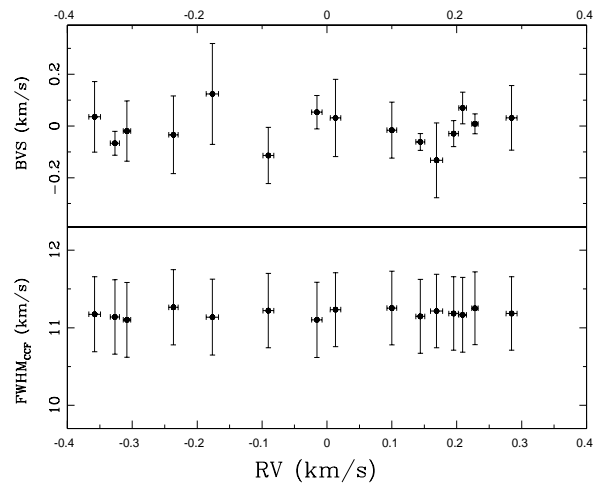
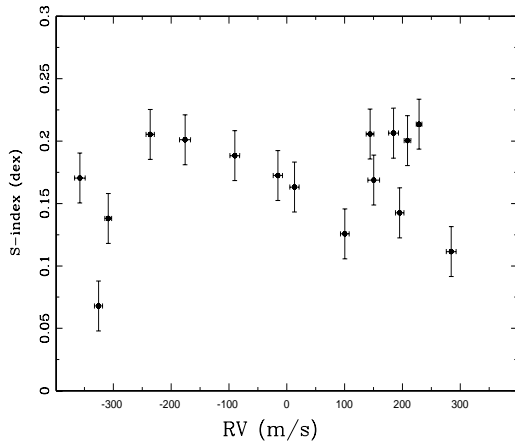


**Fig. 6.** Bisector velocity span (upper panel) and FWHM of the CCF (lower panel) against the RV's measured for HIP 63242. In both cases the CCF's were computed for 11 different orders, covering the wavelength range between  $\sim 5000 - 6000 \text{ \AA}$ . The errorbars correspond to the uncertainty in the mean.

radial velocities. No correlation seems to be present. Based on these stellar activity diagnostics, we can conclude that the most likely explanation for the RV signal observed in HIP 63242 is due to the presence of a substellar companion.

## 5. Summary and conclusions

We computed precision radial velocities using FEROS spectra of the giant star HIP 63242, which have revealed a large periodic signal. We developed a radial velocity computation method that leads to long-term RV precision of  $\sim 3-4 \text{ m s}^{-1}$ , which is much better than was previously obtained with FEROS data. To determine whether these variations are related to intrinsic stellar phenomena (rotational modulation, stellar pulsation or magnetic-related activity), we performed a detailed photometric, line profile and Ca II lines emission analysis. We found no correlation with the RV variations, meaning that the observed radial velocity



Sato, B. et al. 2008, PASJ, 60, 539  
 Schrijver & Pols 1993, A&A, 278, 51  
 Setiawan, J. et al. 2010, Science, 330, 1642  
 Siess, L. & Livio, M. 1999, MNRAS, 308, 1133  
 Sneden, C. 1973, Ph.D. Thesis, ApJ, 184, 839  
 Tonry, J & Davis, M. 1979, AJ, 84, 1511  
 Tuomi, M. et al. 2012, A&A, 551, 79  
 Villaver, E. & Livio, M. 2009, ApJ, 705, 81

**Fig. 7.** S-index variation as described in Jenkins et al. (2008; 2011) against the measured radial velocities for HIP 63242.

signal is likely attributed to an extrinsic mechanism.

According to the best keplerian fit, and assuming a mass for the host star of  $1.54 M_{\odot}$ , we derived a semimajor axis of 0.57 AU for HIP 63242 b, which correspond to the innermost planet detected around a RGB star. The detection of these kind of planets is very important because allow us to better understand what is the effect of the stellar evolution (after the MS) in the orbital properties of planets. In addition, even though close-in planets around intermediate mass stars are rare, more of them can be expected to be detected in the coming years, allowing us to disentangle the effect of the stellar mass from the stellar evolution in their orbits.

*Acknowledgements.* We acknowledge the referee, John A. Johnson for his very useful comments. M.J. and P.R. acknowledge financial support from Fondecyt through grant #1120299. M.J. also acknowledges financial support from ALMA-Conicyt grant #31080027 and from BASAL PFB-06. J.J. acknowledges funding by Fondecyt through grant 3110004 and partial support from CATA (PB06, Conicyt), the GEMINI-CONICYT FUND and from the Comité Mixto ESO-GOBIERNO DE CHILE.

## References

- Alonso, A., Arribas, S. & Martinez-Roger, C. 1999, A&A140, 261  
 Arenou, F., Grenon, M. and Gómez A. 1992, A&A, 258, 104  
 Barnes et al. 2012, MNRAS, 424, 591  
 Bowler, B. P. et al. 2010, A&A, 709, 396  
 Demarque et al. 2004, ApJS, 155, 667  
 Hekker, S. et al. 2006, A&A, 454, 943  
 Figueira, P. et al. 2010, A&A, 513, 8  
 Fitzpatrick M. J. 1993, ASPC, 52, 472  
 Huelamo, N. et al. 2008, A&A, 489, 9  
 Jenkins, J. S. et al. 2008, A&A, 485, 571  
 Jenkins et al. 2009, ApJ, 704, 975  
 Jenkins, J. S. et al. 2011, A&A, 531, 8  
 Jenkins, J. S. et al. 2013, ApJ, 766, 67  
 Johnson, J. A. et al. 2007, A&A, 665, 785  
 Jones, M. I. et al. 2011, A&A, 536, 71  
 Jones, M. I. et al. 2013, in preparation  
 Kaufer, A. et al. 1999, The Messenger 95, 8  
 Kunitomo, M. et al. 2011, ApJ, 737, 66  
 Kurucz, R. L.: ATLAS9 Stellar Atmosphere Programs and 2 km/s Grid, CD-ROM No. 13 (Smithsonian Astrophysical Observatory, Cambridge 1993)  
 Meschiari, S. et al. 2009, PASJ, 121, 1016  
 O'Toole, S. J., Tinney, C. G. & Jones, H. R. A. 2008, MNRAS, 386, 516  
 Queloz, D. et al. 2001, A&A, 379, 279  
 Rutten, R. G. M. & Pylyser, E. 1988, A&A, 191, 227  
 Salasnich, L. et al. 2000, A&A, 361, 1023  
 Sato, B. et al. 2005, PASJ, 57, 97

**Table 3.** Radial velocity measurements of HIP 63242

JD - 2455000	RV ( $\text{m s}^{-1}$ )	error ( $\text{m s}^{-1}$ )
317.5802	209.1	5.9
379.4784	-308.2	5.8
729.4990	-90.3	8.4
744.4786	-358.0	9.1
1056.5393	143.9	6.8
1058.6287	195.2	7.3
1066.5553	228.1	4.9
1099.4790	13.2	8.1
1110.5131	-236.6	7.3
1140.5548	-176.5	9.5
1160.5382	-15.5	8.0
1251.8552	-326.8	7.0
1321.7227	284.6	8.5
1331.7437	168.9	9.3
1342.6957	100.0	7.5